Molecular Crystals and Liquid Crystals

Publication details, including instructions for authors and subscription information:
http://www.tandfonline.com/loi/gmcl20

Impact of Molecular Structure Change on the Hierarchy of Intermolecular Interactions Leading to Polar/Centrosymmetric Crystals

S. Philip Anthony [a], L. Srikanth [a] & T. P. Radhakrishnan [a]

[a] School of Chemistry, University of Hyderabad, Hyderabad, 500 046, India

Version of record first published: 18 Oct 2010

To cite this article: S. Philip Anthony, L. Srikanth & T. P. Radhakrishnan (2002): Impact of Molecular Structure Change on the Hierarchy of Intermolecular Interactions Leading to Polar/Centrosymmetric Crystals, Molecular Crystals and Liquid Crystals, 381:1, 133-150

To link to this article: http://dx.doi.org/10.1080/713738737

Mol. Cryst. Liq. Cryst., Vol. 381, pp. 133–150

1058-725X/02 $12.00 + .00
DOI: 10.1080/10587250290102828

IMPACT OF MOLECULAR STRUCTURE CHANGE ON THE HIERARCHY OF INTERMOLECULAR INTERACTIONS LEADING TO POLAR/CENTROSYMMETRIC CRYSTALS

*S. Philip Anthony, L. Srikanth, and T. P. Radhakrishnan**
School of Chemistry, University of Hyderabad
Hyderabad—500 046, India

Perfectly polar packing of molecules in molecular crystals is of fundamental interest in applications based on the electro-optic effect and piezo, pyro, and ferroelectric effects. The packing of molecules in the crystals of VO(acac)$_2$ (DMAP) complex is investigated and analyzed in the context of the perfect polar packing reported earlier in VO(acac)$_2$ (MP) and Zn(acac)$_2$ (DMAP) complexes. The subtle modification of the ligand is found to effect a drastic change in the molecular geometry between trans *and* cis *in the vanadyl complexes. This in turn affects the hierarchy of intermolecular interactions with dramatic impact on the molecular packing, causing the perfectly polar packing motif in VO(acac)$_2$ (MP) to change to a centrosymmetric one in VO(acac)$_2$ (DMAP).*

Keywords: polar crystal; centrosymmetric crystal; vanadyl complex; *cis-trans* isomers

INTRODUCTION

The bulk properties of molecular materials are intimately linked to the relative orientation and organization of the constituent molecules. For example, the electrical transport in organic molecular conductors based on charge transfer complexes critically depends on the interplanar distances and π-orbital overlaps of the electron donor/acceptor molecules [1]. Magnetic interactions and hence the cooperative magnetism in molecular magnets can change drastically when the mutual disposition of the molecular radicals is

Received 12 April 2002; accepted 19 April 2002.

Financial support from the Department of Science and Technology, New Delhi (Swarnajayanti Fellowship) and the use of the National Single Crystal Diffractometer Facility funded by the DST at the School of Chemistry, University of Hyderabad are gratefully acknowledged. S. Philip Anthony thanks the Council of Scientific and Industrial Research, New Delhi for a junior research fellowship.

*Corresponding author. Fax: 91-40-301-2460, Email: tprsc@uohyd.ernet.in

altered [2]. In quadratic nonlinear optical (NLO) crystals, beyond the necessary prerequisite of noncentrosymmetric lattice structure, the orientation of the molecular hyperpolarizability tensor components determines the bulk nonlinear response. While the phase-matching conditions and the crystal system symmetry dictate the optimal relative orientation between molecules for efficient second harmonic generation [3], the ideal organization of molecules for phenomena such as the electro-optic effect is a perfectly polar assembly with all the molecular dipoles aligned parallel [4]. Such molecular assemblies are of general interest in other applications such as ferroelectricity, pyroelectricity, and piezoelectricity as well [5].

A variety of molecular features have been exploited to tailor the desired assembly of molecular crystals for NLO applications such as second harmonic generation. Intermolecular H-bonds [6], internal cancellation of molecular dipole moment [7], molecular chirality [8], and the balance of electrostatic and dispersion energies [9] are some of the approaches developed to achieve noncentrosymmetric crystal lattices. For applications such as the electro-optic effects, parallel orientation of the molecular dipoles embedded in polymer films can be achieved through electric field poling; however depoling effects are often a practical problem [10]. Perfectly polar molecular crystals are rare. Strategies developed towards this goal include the salt methodology [11], cocrystallization techniques [12], host-guest inclusion compounds [13], and open framework systems [14]. A stochastic model has been developed to gain insight into the growth of polar structures in inclusion compounds [13].

The approaches listed above for the polar organization of NLO chromophores require the involvement of a supporting structure based on the host polymer or framework lattice, counterion or cocrystallization partner. This invariably leads to a lower density of the NLO active component in the bulk material. It is therefore desirable to develop single component lattices with a perfectly polar alignment of the constituent molecular dipoles. Strong and directional H-bonding has been effectively exploited in self-assembly processes, leading to highly anisotropic nanostructures and thin films [15]. We have recently realized perfectly polar single component crystal formation in some simple metal-organic compounds [16]. The polar ordering, described as a case of "self-poling," was explained on the basis of a hierarchy of highly anisotropic intermolecular interactions in the 3-dimensional crystal lattice, in the spirit of the stochastic model referred to above. The strong dipole-dipole interactions of these push-pull (D-A) molecules lead to oriented chains along one of the crystal axes. The weak or negligible lateral interactions coupled with the different D$\cdots$D and A$\cdots$A intermolecular interaction energies lead to parallel orientation of the chains, resulting in an overall perfectly polar assembly.

Metal atoms coordinated by substituted pyridine ligands are potentially interesting candidates for quadratic NLO applications since these push-pull

molecules can be tuned to achieve appreciable hyperpolarizability. We have explored several modifications on the prototypical system, bis(acetylacetonato)(4-dimethylaminopyridyl)zinc(II), Zn(II)(acac)$_2$(DMAP) (ZNDA), and found that the same kind of polar ordering is achieved in crystals of bis(acetylacetonato)(4-morpholinopyridyl)zinc(II) [16]. We have now investigated the replacement of Zn(II) by the vanadyl ion; we report the crystal structure of bis(acetylacetonato)(4-dimethylaminopyridyl)vanadyl(II), VO(II)(acac)$_2$(DMAP)(VOAD) and carry out a systematic analysis of the crystal packing. Earlier reports have dwelled on the molecular structures of vanadyl complexes with acac and different pyridine-based ligands and addressed issues related to *cis* and *trans* coordination around vanadium (IV). We present in this paper the dramatic effect of minor molecular structural changes on the bulk molecular assembly of these vanadyl complexes leading to perfectly polar or centrosymmetric lattices. Utilizing the model of the ZNDA complex, we analyze the molecular features that lead to such changes in the packing patterns, which is of critical relevance to the NLO attributes of the bulk material.

EXPERIMENTAL AND COMPUTATIONAL

VO(II)(acac)$_2$ was synthesized following reported procedure [17]. Methanol solutions of VO(II)(acac)$_2$ and 4-dimethylaminopyridine (DMAP) were mixed in 1:1 ratio; slow evaporation yielded green crystals of VOAD.

X-ray diffraction data were collected on an Enraf-Nonius MACH3 diffractometer. MoK_α radiation with a graphite crystal monochromator in the incident beam was used. Data was reduced using Xtal3.4 [18]; Lorentz and polarization corrections were included. Using the SHELX-97 [19] program, the position of the unique V atom was determined from a Patterson map and the remaining non-H atoms were located using the difference Fourier map. After several cycles of refinement the positions of the hydrogen atoms were calculated and added to the refinement process. Graphics were handled using ORTEX6a [20]. Details of data collection, solution and refinement, fractional coordinates with anisotropic thermal parameters, and full lists of bond lengths and angles are presented in the Appendix.

Charge density on the N atom of the pyridine ligands were calculated using semiempirical AM1 [21] and ab initio [22] methods through full geometry optimization of the molecules.

RESULTS AND DISCUSSION

Single crystal X-ray diffraction analysis of VOAD (Table 1) revealed the *cis* geometry of the molecule (Figure 1); the angle between the DMAP

TABLE 1 Crystallographic Data for VOAD

	VOAD
Molecular formula	$C_{17}H_{24}N_2O_5V$
Formula weight	387.32
Crystal system	Triclinic
Space group	$P\bar{1}$ (No.2)
a (Å)	8.057(18)
b (Å)	11.520(13)
c (Å)	11.716(10)
α (deg.)	71.00(7)
β (deg.)	69.64(10)
γ (deg.)	71.30(12)
Z	2
$\rho_{calc.}$(g cm^{-3})	1.372
λ (Å)	0.71703
μ (cm^{-1})	5.57
Absorption correction	Empirical; $T_{min} = 0.8272$, $T_{max} = 0.9991$
Number of unique reflections	4075
Number of reflections with $I \geq 2\sigma_I$	1783
Number of parameters	232
GOF	1.020
R (for $I \geq 2\sigma_I$)	0.0737
wR^2	0.1473

nitrogen-vanadium bond and the vanadyl (V=O) bond is 95.0°. The significant bond lengths and angles in the molecule are collected in Table 2. The length of the V-N bond to the DMAP ligand and the V=O bond of the vanadyl group are respectively 2.153 and 1.600 Å. The lengths of the V-O bonds to the acac ligands are 1.970, 1.990, 2.033, and 2.151Å. The last two are the bonds ***trans*** to the DMAP and oxo group, respectively, and are clearly longer than the other two. The various V-O bond lengths closely parallel those reported for the $VO(acac)_2$(isopropoxy) complex [23]. The two long V-O bonds clearly suggest the influence of the so-called '***trans***' directing ligands. The classical explanation [24] of the ***cis*** orientation of these two ***trans***-directing ligands appear to prevail in the case of VOAD.

We have searched the Cambridge Structural Database [25] for the molecular structures and packing of simple mononuclear $VO(acac)_2L$ type complexes. Structures have been reported for systems with L = 4-phenylpyridine (PP) [26], pyridine (P) [27], 4-methylpyridine (MP) [28], and isopropoxy (IP) [23]. The PP and IP complexes adopt a ***cis*** structure as in VOAD whereas the MP and P complexes adopt a ***trans*** structure.

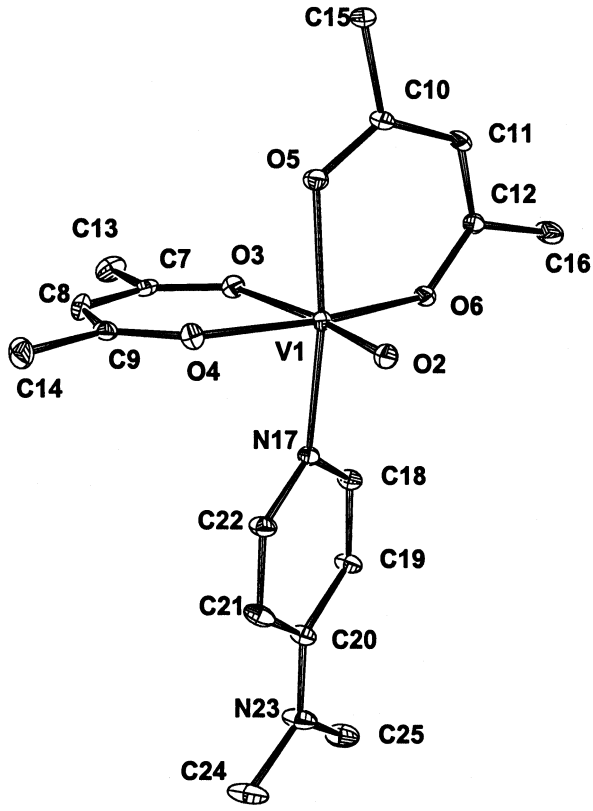

FIGURE 1 Molecular structure of VOAD from single crystal X-ray crystallographic analysis. H atoms are omitted for clarity. Ten percent probability thermal ellipsoids are shown.

The basicity of the ligand L appears to be the primary factor determing the *cis/trans* preference. A semiquantitative idea about the basicity of the ligand is provided by the calculated charge density on the N atom of the pyridine ligands or the O atom of the isopropoxy ligand. These values, computed using quantum chemical methods, are collected in Table 3. Pyridine and 4-methylpyridine have low negative charge on N and form *trans* complex. Isopropoxy and DMAP have strong negative charge on the ligating atom, leading to *cis* geometry of the complex. The atomic charge on the N atom of 4-phenylpyridine is rather small; therefore considerations other than the basicity, perhaps steric factors or crystal packing considerations, appear to give rise to the *cis* geometry of the corresponding vanadyl complex.

TABLE 2 Significant Bond Lengths and Angles in VOAD

Bond	Length (Å)
V(1)-O(2)	1.600(13)
V(1)-O(6)	1.970(12)
V(1)-O(4)	1.990(13)
V(1)-O(5)	2.033(13)
V(1)-N(17)	2.153(14)
V(1)-O(3)	2.151(13)
O(3)-C(7)	1.26(2)
O(4)-C(9)	1.28(2)
O(5)-C(10)	1.30(2)
O(6)-C(12)	1.26(2)
N(17)-C(18)	1.31(2)
N(17)-C(22)	1.36(2)
N(23)-C(20)	1.36(2)
N(23)-C(25)	1.43(3)
N(23)-C(24)	1.49(3)
C(7)-C(8)	1.40(3)
C(7)-C(13)	1.50(3)
C(8)-C(9)	1.34(3)
C(9)-C(14)	1.49(3)
C(10)-C(11)	1.40(3)
C(10)-C(15)	1.49(2)
C(11)-C(12)	1.36(3)
C(12)-C(16)	1.51(3)
C(18)-C(19)	1.36(3)
C(19)-C(20)	1.39(3)
C(20)-C(21)	1.41(3)
C(21)-C(22)	1.34(3)
Bond-bond	**Angle (°)**
O(2)-V(1)-O(6)	99.6(6)
O(2)-V(1)-O(4)	94.1(6)
O(6)-V(1)-O(4)	166.3(5)
O(2)-V(1)-O(5)	99.3(6)
O(6)-V(1)-O(5)	88.8(5)
O(4)-V(1)-O(5)	88.0(5)
O(2)-V(1)-N(17)	95.0(6)
O(6)-V(1)-N(17)	88.4(5)
O(4)-V(1)-N(17)	91.4(6)
O(5)-V(1)-N(17)	165.7(5)
O(2)-V(1)-O(3)	175.0(6)
O(6)-V(1)-O(3)	83.7(5)
O(4)-V(1)-O(3)	82.7(5)
O(5)-V(1)-O(3)	84.5(5)
N(17)-V(1)-O(3)	81.2(5)
C(7)-O(3)-V(1)	129.2(12)
C(9)-O(4)-V(1)	133.5(12)

(Continued)

TABLE 2 Continued

Bond-bond	Angle (°)
C(10)-O(5)-V(1)	124.2(12)
C(12)-O(6)-V(1)	128.2(12)
C(18)-N(17)-C(22)	114.8(15)
C(18)-N(17)-V(1)	125.9(12)
C(22)-N(17)-V(1)	119.2(12)
C(20)-N(23)-C(25)	123.0(18)
C(20)-N(23)-C(24)	120.5(18)
C(25)-N(23)-C(24)	116.4(18)
O(3)-C(7)-C(8)	124.5(17)
O(3)-C(7)-C(13)	117.2(18)
C(8)-C(7)-C(13)	118.2(18)
C(9)-C(8)-C(7)	124.2(18)
O(4)-C(9)-C(8)	125.7(17)
O(4)-C(9)-C(14)	115.3(18)
C(8)-C(9)-C(14)	119.0(19)
O(5)-C(10)-C(11)	125.5(16)
O(5)-C(10)-C(15)	114.6(17)
C(11)-C(10)-C(15)	119.7(17)
C(10)-C(11)-C(12)	124.5(17)
O(6)-C(12)-C(11)	125.7(18)
O(6)-C(12)-C(16)	115.2(17)
C(11)-C(12)-C(16)	119.0(17)
N(17)-C(18)-C(19)	124.9(17)
C(18)-C(19)-C(20)	120.7(19)
C(21)-C(20)-N(23)	122.6(18)
C(21)-C(20)-C(19)	114.7(17)
N(23)-C(20)-C(19)	122.6(19)
C(20)-C(21)-C(22)	119.9(18)
N(17)-C(22)-C(21)	124.9(18)

VOAD packs into a centrosymmetric crystal lattice belonging to the $P\bar{1}$ space group. The views approximately along the ***a*** axis and perpendicular to the ***ac*** plane are shown in Figure 2. Weak intermolecular interactions of the C-H $\cdots$ O = V [29] and C-H $\cdots$ O [30] type appear to stabilize the lattice

TABLE 3 Computed Atomic Charges on the Coordinating Atom of the Various Ligands, L in $VO(acac)_2L$; Results from Semiempirical AM1 and PM3 and ab initio B3LYP/6-31G* Calculations are Shown

Ligand, L	AM1	PM3	B3LYP/6-31G*
P	−0.138	−0.079	−0.406
MP	−0.142	−0.086	−0.411
PP	−0.138	−0.081	−0.409
DMAP	−0.170	−0.112	−0.428
IP	−0.745	−0.812	−0.751

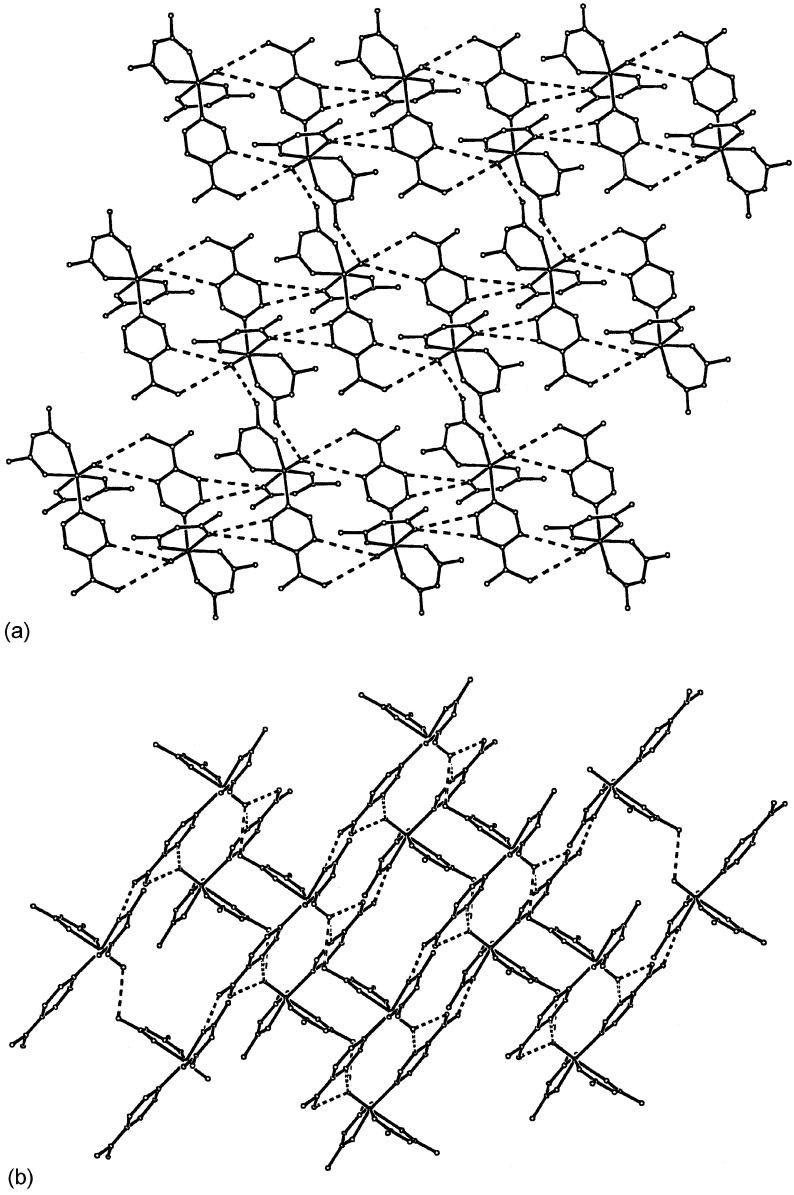

FIGURE 2 Packing of molecules of VOAD crystals viewed approximately (**a**) along the *a* axis (broken lines indicate the noncovalent O2 ··· C15, O2 ··· C21, O2 ··· C24, O3 ··· C18, and O3 ··· C19 interactions) and (**b**) perpendicular to the *ac* plane (broken lines indicate the noncovalent O2 ··· C13, O2 ··· C21, O2 ··· C24, and O5 ··· C25 interactions).

structure and more significantly induce the centrosymmetric packing as discussed below. Several noncovalent interactions leading to short C···O distances in the range 3.49 to 3.64 Å are observed. It may be noted that functionalities required for strong H-bond interactions are not present in the VOAD molecule.

A comparison of the crystal packing in VOAD with the other $VO(acac)_2L$ complexes is instructive. The crystallographic space groups of the earlier four complexes and VOAD are collected in Table 4. It is interesting to note that only the MP complex forms a perfectly polar structure similar to the one found in ZNDA [16]; a schematic representation of the polar lattice is shown in Figure 3. The *trans* structure of this complex would give rise to an appreciable ground state dipole moment. This encourages strong head-to-tail interaction, resulting in chains of molecular dipoles (D-A···D-A···D-A). Given the molecular structure, potential intermolecular D···D and A···A interaction energies are likely to be very different. The shape and structure of the complex leads to effective insulation of lateral intermolecular interactions between the dipole chains. The situation is similar to that found in ZNDA and satisfies the requirements of the stochastic model for polarity generation in molecular crystals [13]. In the case of $VO(acac)_2P$ complex, even though the molecular geometry is *trans,* the molecular dipole moment is likely to be weaker than that of the MP analog. This would result in lower anisotropy in the intermolecular interactions, and this factor most likely leads to the centrosymmetric packing in the crystal. A careful analysis of the crystal structure of VOAD shows fairly similar intermolecular interactions in different directions (Figure 2). Since the molecule has *cis* geometry the dipole moment will be small. The strong hierarchy of interactions observed in ZNDA or in $VO(acac)_2MP$ cannot therefore occur in the case of VOAD. This explains the absence of a polar ordering in this crystal. The minor modification of the group at the 4-position of the pyridine ligand from methyl to dimethylamino leads to a strong change in the molecular structure and, as a consequence of this, to a drastic change in the crystal packing all the way from a perfectly polar

TABLE 4 Molecular Geometry and Space Group of the Various $VO(acac)_2L$ Complexes

Ligand, L	*cis/trans*	Space group	Ref.
P	*trans*	C2/c	[27]
MP	*trans*	Cm	[28]
PP	*cis*	C2/c	[26]
IP	*cis*	$P2_1/n$	[23]
DMAP	*cis*	$P\bar{1}$	This work

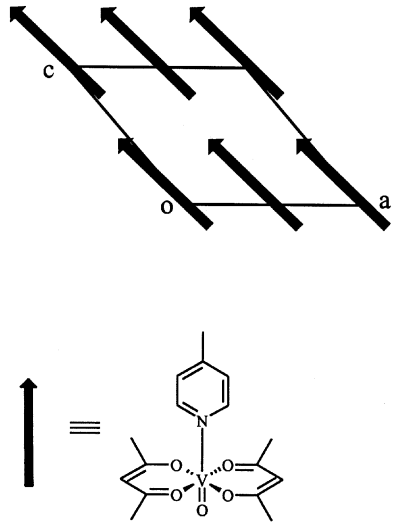

FIGURE 3 Schematic drawing of the polar lattice structure in the $VO(acac)_2(MP)$ complex [28].

structure to a completely centrosymmetric packing! Similar logic as in the case of VOAD explains the packing observed in the IP and PP complexes; the *cis* geometry in both cases leads to less anisotropic intermolecular interactions, resulting in a centrosymmetric lattic structure.

CONCLUSION

The current study places the crystallographic investigation of the VOAD complex in the general context of the molecular and crystal structures of $VO(acac)_2L$ complexes, which are potential candidates to develop highly polar crystal lattices of interest in a variety of materials applications. The dramatic impact of minor molecular structure variation of L on the molecular geometry of the coordination complex, and more significantly on the crystal packing, are clearly delineated. The minor modification of the ligand causes *trans-cis* structural change in the complex, a direct consequence of the electronic structure influence. The impact of this on the hierarchy of intermolecular interactions in 3-D is profound, leading to a dramatic switching from a polar order to centrosymmetric packing. We have developed new Zn complexes where the polar order of the molecular packing is preserved and structural and nonlinear optical studies on crystalline powders and thin films of these thermally stable materials are in progress.

REFERENCES

[1] (a) Torrance, J. B. (1985). *Mol. Cryst. Liq. Cryst.*, *126*, 55–67.
(b) Torrance, J. B. (1979). *Acc. Chem. Res.*, *12*, 79–86.

[2] (a) Takahashi, M., Turek, P., Nakazawa, Y., Tamura, M., Nozawa, K., Shiomi, D., Ishikawa, M., & Kinoshita, M. (1991). *Phys. Rev. Lett.*, *67*, 746–748.
(b) Allemand, P. M., Srdanov, G., & Wudl, F. (1990). *J. Am. Chem. Soc.*, *112*, 9391–9392.
(c) McConnell, H. M. (1963). *J. Chem. Phys.*, *39*, 1910.

[3] (a) Zyss, J., & Chemla, D. S. (1989). In D. S. Chemla & J. Zyss (Eds.), *Nonlinear Optical Properties of Organic Molecules and Crystals*, Vol. 1 (p. 23). New York: Academic Press.
(b) Zyss, J., & Oudar, J. L. (1982). *Phys. Rev. A*, *26*, 2028–2048.

[4] (a) Bosshard, C., & Günter, P. (1997). In S. Miyata & H. S. Nalwa (Eds.), *Nonlinear Optics of Organic Molecular and Polymeric Materials* (p. 391). Boca Raton, FL: CRC Press.
(b) Chemla, D. S., & Zyss, J. (Eds.) (1989). *Nonlinear Optical Properties of Organic Molecules and Crystals*, Vols. 1, 2. New York: Academic Press.

[5] Weber, M. J., ed. (1995). *Handbook of Laser Science and Technology*, Supplement 2: Optical Materials, Boca Raton, FL: CRC Press.

[6] (a) Ravi, M., Gangopadhyay, P., Rao, D. N., Cohen, S., Agranat, I., & Radhakrishnan, T. P. (1998). *Chem. Mater.*, *10*, 2371–2377.
(b) Bernstein, J., Davis, R. E., Shimoni, L. & Chang, N. (1995). *Angew. Chem. Int. Ed. Engl.*, *34*, 1555–1573.
(c) Desiraju, G. R. (1989). *Crystal Engineering: The Design of Organic Solids*, Amsterdam: Elsevier.

[7] (a) Twieg, R., Azema, A., Jain, K., & Cheng, Y. Y. (1982). *Chem. Phys. Lett.*, *92*, 208–211.
(b) Sigelle, M., Zyss, J. & Hierle, R. (1982). *J. Non-Cryst. Solids*, *47*, 287–289.
(c) Zyss, J., Chemla, D. S., & Nicoud, J. F. (1981). *J. Chem. Phys.*, *74*, 4800–4811.

[8] (a) Gangopadhyay, P., & Radhakrishnan, T. P. (2001). *Angew. Chem. Int. Ed. Engl.*, *40*, 2451–2455.
(b) Ukachi, T., & Sugiyama, T. (1993). *J. Opt. Soc. Am. B*, *10*, 1372–1378.
(c) Eaton, D. F. (1991). *Science*, *253*, 281–287.
(d) Rieckoff, K., & Peticolas, W. F. (1965). *Science*, *147*, 610–611.

[9] (a) Gangopadhyay, P., & Radhakrishnan, T. P. (2000). *Chem. Mater.*, *12*, 3362–3368.
(b) Sharma, S., & Radhakrishnan, T. P. (2000). *Mol. Cryst. Liq. Cryst.*, *338*, 257–269.
(c) Gangopadhyay, P., Sharma, S., Rao, A. J., Rao, D. N., Cohen, S., Agranat, I., & Radhakrishnan, T. P. (1999). *Chem. Mater.*, *11*, 466–472.
(d) Gangopadhyay, P., Rao, S. V., Rao, D. N., & Radhakrishnan, T. P. (1999). *J. Mater. Chem.*, *9*, 1699–1705.

[10] Miyata, S., & Sasabe, H. eds., 1997. *Poled Polymers and their Applications to SHG and EO Devices*. Amsterdam: Gordon and Breach.

[11] (a) Marder, S. R., Perry, J. W., & Yakymyshyn, C. P. (1994). *Chem. Mater.*, *6*, 1137–1147.
(b) Marder, S. R., Perry, J. W., & Schaefer, W. P. (1989). *Science*, *245*, 626–628.

[12] Wong, M. S., Pan, F., Bösch, M., Spreiter, R., Bosshard, C., Günter, P., & Gramlich, V. (1998). *J. Opt. Soc. Am. B*, *15*, 426–431.

[13] (a) Hulliger, J., Roth, S. W., Quintel, A., & Bebie, H. (2000). *J. Solid State Chem.*, *152*, 49–56.
(b) Hulliger, J., Langley, P. J., Quintel, A., Rechsteiner, P., & Roth, S. W. (1999). In J. Veciana, C. Rovira, & Amabilino D. B., (Eds.), *Supramolecular Engineering of Synthetic Metallic Materials*, (p. 67–81) The Netherlands: Kluwer.

(c) Quintel, A., Hulliger, J., & Wübbenhorst, M. (1998). *J. Phys. Chem. B*, *102*, 4277–4283.
(d) König, O., Bürgi, H.-B., Armbruster, T., Hulliger, J., & Weber, T. (1997). *J. Am. Chem. Soc.*, *119*, 10632–10640.
(e) Hoss, R., König, O., Kramer-Hoss, V., Berger, U., Rogin, P., & Hulliger, J. (1996). *Angew. Chem., Int. Ed. Engl.*, *35*, 1664–1666.
(f) Hulliger, J., König, O., & Hoss, R. (1995). *Adv. Mater.*, *7*, 719–721.
[14] Holman, K. T., Pivovar, A. M., & Ward, M. D. (2001). *Science*, *294*, 1907–1911.
[15] Cai, C., Bösch, M., Tao, Y., Müller, B., Gan, Z., Kündig, A., Bosshard, C., Liakatas, I., Jäger, M., & Günter, P. (1998). *J. Am. Chem. Soc.*, *120*, 8563–8564.
[16] Philip Anthony, S., & Radhakrishnan, T. P. (2001). *Chem. Commun.*, 931–952.
[17] Rowe, R. A., & Jones, M. M. (1957). *Inorg. Synth.*, *5*, 115.
[18] Hall, S. R., King, G. S. D., & Stewart, J. M., eds., (1995). *Xtal3.4*, University of Western Australia: Crawely.
[19] Sheldrick, G. M. (1997). *SHELX-97*, University of Göttingen: Göttingen.
[20] McArdle, P. (1995). *J. Appl. Cryst.*, *28*, 65.
[21] (a) Dewar, M. J. S., Zoebisch, E. G., Healy, E. F., & Stewart, J. J. P. (1985). *J. Am. Chem. Soc. 107*, 3902–3907.
(b) *MOPAC93*, © Fujitsu Inc.
[22] Frisch, M. J., Trucks, G. W., Schlegel, H. B., Gill, P. M. W., Johnson, B. G., Robb, M. A., Cheeseman, J. R., Keith, T., Petersson, G. A., Montgomery, J. A., Raghavachari, K., Al-Laham, M. A., Zakrzewski, V. G., Ortiz, J. V., Foresman, J. B., Cioslowski, J., Stefanov, B. B., Nanayakkara, A., Challacombe, M., Peng, C. Y., Ayala, P. Y., Chen, W., Wong, M. W., Andres, J. L., Replogle, E. S., Gomperts, R., Martin, R. L., Fox, D. J., Binkley, J. S., Defrees, D. J., Baker, J., Stewart, J. P., Head-Gordon, M., Gonzalez, C., & Pople J. A. (1995). *Gaussian94*, Revision D.2, Gaussian, Inc., Pittsburgh, PA.
[23] Jiang, F., Anderson, O. P., Miller, S. M., Chen, J., Mahroof-Tahir, M., & Crans, D. C. (1998). *Inorg. Chem.*, *37*, 5439–5451.
[24] (a) Sun, Y., James, B. R., Rettig, S. J., & Orvig, C. (1996). *Inorg. Chem.*, *35*, 1667–1673.
(b) Scheidt, W. R. (1973). *Inorg. Chem.*, *12*, 1758.
[25] Cambridge Structural Database, Version 5.23. (April 2002). Cambridge Crystallographic Data Center, Cambridge.
[26] Caira, M. R., Haigh, J. M., & Nassimbeni, L. R. (1972). *Inorg. Nucl. Chem. Lett.*, *8*, 109 (April 2002).
[27] (a) Meicheng, S., Lifeng, W., & Youqi, T. (1984). *Kexue Tongabao*, *29*, 759–764.
(b) Cambridge Structural Database, Cambridge Crystallographic Data Center, Cambridge—Refcode: CUCWUS.
[28] (a) Meicheng, S., Lifeng, W., & Zeying, Z. (1983). *Huaxue Xuebao (Acta Chim. Sinica)*, *41*, 985.
(b) Cambridge Structural Database, Cambridge Crystallographic Data Center, Cambridge—Refcode: CEXVEG.
[29] Pal, S. N., Radhika, K. R., & Pal, S. (2001). *Z. Anorg. Allg. Chem.*, *627*, 1631–1637.
[30] Desiraju, G. R. (1996). *Acc. Chem. Res.*, *29*, 441–449.

APPENDIX

Supplementary Information for "Impact of Molecular Structure Change on the Hierarchy of Intermolecular Interactions Leading to Polar/Centrosymmetric Crystals"

CRYSTAL STRUCTURE OF VOAD

Structure Determination

Single crystal X-ray data were measured on an ENRAF-NONIUS MACH2 diffractometer. MoK_α ($\lambda = 0.71073$ Å) radiation with a graphite crystal monochromator in the incident beam was used. The standard CAD4 centering, indexing, and data collection programs were used. The unit cell dimensions were obtained by a least-squares fit of 24 centered reflections in the neighborhood of $\theta = 10°$. Intensity data were collected using the ω scan method at a scan speed of 4.12°/min to a maximum 2θ of 50°. The scan width, $\Delta\theta$ for each reflection, was $1.00 + 0.35 \tan\theta$. During data collection the intensities of three standard reflections were monitored every 1.5 h; no decay was observed. Three orientation standards were monitored every 250 reflections to check the effects of crystal movement. Intensities were corrected for Lorentz and polarization effects. Using the SHELXS-97 program, the V atom was found by Patterson map and the remaining non-H atoms were obtained from the Fourier map. All non-H atoms were refined anisotropically. H atoms were added at idealized positions for structure factor calculation but were not refined (all computations were carried out on a Pentium PC using SHELXL-97). Refinement proceeded to convergence by minimizing $\sum w(F_o^2 - F_c^2)$. A final difference Fourier synthesis map showed the largest difference peak and hole to be very small. The R indices are calculated as $R = \sum |(|F_o| - |F_c|)| / \sum |F_o|$ and $wR^2 = [\sum w(F_o^2 - F_c^2)^2 / \sum (F_o^2)^2]^{1/2}$. The pertinent crystallographic data are provided in Tables 1 to 6.

TABLE 1 Crystal Data and Structure Refinement for VOAD

Identification code	VOAD
Molecular formula	$C_{17}H_{24}N_2O_5V$
Formula weight	387.32
Crystal system	Triclinic
Space group	$P\bar{1}$ (No.2)
Color and appearance	Green cube
Dimensions (mm × mm × mm)	0.26 × 0.24 × 0.24
a (Å)	8.057(18)
b (Å)	11.520(13)
c (Å)	11.716(10)
α (deg.)	71.00(7)
β (deg.)	69.64(10)
γ (deg.)	71.30(12)
Z	2
μ (cm^{-1})	5.57
Temperature (K)	293(2)
λ (Å)	0.71073
2θ range (deg.)	1.91–26.99
Absorption correction	Empirical—psi-scan
T_{min}	0.9991
T_{max}	0.8272
Refinement method	Full matrix Least Squares on F^2
No. of unique reflections	4075
No. of reflections with $I \geq 2\sigma_I$	1783
No. of parameters	232
GOF	1.020
$\rho_{calc.}$/g cm^{-3}	1.372
R [for $I \geq 2\sigma_I$]; wR^2	0.0737; 0.1473
R (for all data); wR^2	0.1734; 0.2023
Largest diff. peak and hole (e. $Å^{-3}$)	0.37, −0.27

TABLE 2 Atomic Coordinates ($\times 10^4$) and Equivalent Isotropic Displacement Parameters ($Å^2 \times 10^3$) for VOAD. U_{eq} is Defined as One Third of the Trace of the Orthogonalized U_{ij} Tensor

	x	y	z	U_{eq}
V(1)	6135(4)	8150(3)	7870(3)	40(1)
O(2)	4853(17)	7595(12)	7508(12)	49(3)
O(3)	7885(17)	8748(11)	8482(12)	48(3)
O(4)	8135(18)	6594(11)	7855(12)	57(3)
O(5)	7556(17)	8912(11)	6117(12)	58(3)
O(6)	4570(16)	9847(11)	7958(11)	51(3)
N(17)	5031(19)	7538(13)	9865(13)	48(3)
N(23)	2570(3)	6136(17)	13652(17)	86(6)
C(7)	9390(3)	8155(19)	8697(16)	48(4)

(Continued)

TABLE 2 Continued

	x	y	z	U_{eq}
C(8)	10280(3)	6926(19)	8561(19)	60(5)
C(9)	9640(3)	6242(17)	8153(16)	51(5)
C(10)	6970(3)	10012(18)	5440(17)	55(5)
C(11)	5420(3)	10920(17)	5860(19)	54(5)
C(12)	4390(2)	10811(16)	7072(18)	59(4)
C(13)	10260(3)	8800(2)	9180(2)	67(6)
C(14)	10730(3)	4950(2)	8020(2)	82(7)
C(15)	8180(3)	10330(2)	4146(18)	68(6)
C(16)	2930(3)	11940(2)	7440(2)	72(7)
C(18)	4060(3)	8274(16)	10630(17)	52(4)
C(19)	3210(3)	7869(18)	11860(19)	61(5)
C(20)	3360(3)	6585(18)	12415(18)	57(5)
C(21)	4450(3)	5785(18)	11610(19)	64(6)
C(22)	5240(3)	6283(18)	10407(18)	59(5)
C(24)	2900(4)	4750(2)	14230(2)	89(9)
C(25)	1500(4)	6940(2)	14480(2)	85(7)

TABLE 3 Significant Bond Lengths in VOAD

Bond	Length (Å)
V(1)-O(2)	1.600(13)
V(1)-O(6)	1.970(12)
V(1)-O(4)	1.990(13)
V(1)-O(5)	2.033(13)
V(1)-N(17)	2.153(14)
V(1)-O(3)	2.151(13)
O(3)-C(7)	1.26(2)
O(4)-C(9)	1.28(2)
O(5)-C(10)	1.30(2)
O(6)-C(12)	1.26(2)
N(17)-C(18)	1.31(2)
N(17)-C(22)	1.36(2)
N(23)-C(20)	1.36(2)
N(23)-C(25)	1.43(3)
N(23)-C(24)	1.49(3)
C(7)-C(8)	1.40(3)
C(7)-C(13)	1.50(3)
C(8)-C(9)	1.34(3)
C(9)-C(14)	1.49(3)
C(10)-C(11)	1.40(3)
C(10)-C(15)	1.49(2)
C(11)-C(12)	1.36(3)
C(12)-C(16)	1.51(3)
C(18)-C(19)	1.36(3)
C(19)-C(20)	1.39(3)
C(20)-C(21)	1.41(3)
C(21)-C(22)	1.34(3)

TABLE 4 Significant Bond Angles in VOAD

Bond-bond	Angle (°)
O(2)-V(1)-O(6)	99.6(6)
O(2)-V(1)-O(4)	94.1(6)
O(6)-V(1)-O(4)	166.3(5)
O(2)-V(1)-O(5)	99.3(6)
O(6)-V(1)-O(5)	88.8(5)
O(4)-V(1)-O(5)	88.0(5)
O(2)-V(1)-N(17)	95.0(6)
O(6)-V(1)-N(17)	88.4(5)
O(4)-V(1)-N(17)	91.4(6)
O(5)-V(1)-N(17)	165.7(5)
O(2)-V(1)-O(3)	175.0(6)
O(6)-V(1)-O(3)	83.7(5)
O(4)-V(1)-O(3)	82.7(5)
O(5)-V(1)-O(3)	84.5(5)
N(17)-V(1)-O(3)	81.2(5)
C(7)-O(3)-V(1)	129.2(12)
C(9)-O(4)-V(1)	133.5(12)
C(10)-O(5)-V(1)	124.2(12)
C(12)-O(6)-V(1)	128.2(12)
C(18)-N(17)-C(22)	114.8(15)
C(18)-N(17)-V(1)	125.9(12)
C(22)-N(17)-V(1)	119.2(12)
C(20)-N(23)-C(25)	123.0(18)
C(20)-N(23)-C(24)	120.5(18)
C(25)-N(23)-C(24)	116.4(18)
O(3)-C(7)-C(8)	124.5(17)
O(3)-C(7)-C(13)	117.2(18)
C(8)-C(7)-C(13)	118.2(18)
C(9)-C(8)-C(7)	124.2(18)
O(4)-C(9)-C(8)	125.7(17)
O(4)-C(9)-C(14)	115.3(18)
C(8)-C(9)-C(14)	119.0(19)
O(5)-C(10)-C(11)	125.5(16)
O(5)-C(10)-C(15)	114.6(17)
C(11)-C(10)-C(15)	119.7(17)
C(10)-C(11)-C(12)	124.5(17)
O(6)-C(12)-C(11)	125.7(18)
O(6)-C(12)-C(16)	115.2(17)
C(11)-C(12)-C(16)	119.0(17)
N(17)-C(18)-C(19)	124.9(17)
C(18)-C(19)-C(20)	120.7(19)
C(21)-C(20)-N(23)	122.6(18)
C(21)-C(20)-C(19)	114.7(17)
N(23)-C(20)-C(19)	122.6(19)
C(20)-C(21)-C(22)	119.9(18)
N(17)-C(22)-C(21)	124.9(18)

TABLE 5 Anisotropic Displacement Parameters ($Å^2 \times 10^3$) for VOAD: the Anisotropic Displacement Factor Exponent Takes the Form: $-2\,\pi^2\,[h^2\,a^{*2}U_{11}+\cdots+2\,h\,k\,a^*\,b^*\,U_{12}]$

	U_{11}	U_{22}	U_{33}	U_{23}	U_{13}	U_{12}
V(1)	35(2)	40(2)	44(2)	−14(1)	−8(1)	−4(1)
O(2)	41(7)	57(7)	52(8)	−21(6)	−10(6)	−9(6)
O(3)	47(8)	52(7)	51(8)	−27(6)	−9(6)	−9(6)
O(4)	61(8)	46(7)	71(8)	−17(6)	−28(7)	−7(6)
O(5)	61(8)	51(7)	50(7)	−3(6)	−8(6)	−17(6)
O(6)	48(7)	42(7)	51(7)	4(6)	−12(6)	−12(5)
N(17)	58(8)	44(8)	45(8)	−2(6)	−17(7)	−24(6)
N(23)	128(16)	60(11)	46(10)	−5(8)	5(10)	−27(11)
C(7)	42(10)	73(12)	31(9)	−11(8)	−2(8)	−26(9)
C(8)	35(10)	66(13)	74(13)	−12(11)	−18(9)	−5(9)
C(9)	55(11)	49(10)	36(9)	−6(8)	−2(8)	−8(9)
C(10)	71(12)	46(11)	41(9)	1(8)	−14(9)	−18(9)
C(11)	67(12)	39(10)	46(11)	1(9)	−15(10)	−9(9)
C(12)	61(10)	43(10)	68(12)	4(8)	−12(9)	−29(8)
C(13)	48(14)	88(17)	74(14)	−40(12)	−7(11)	−18(13)
C(14)	71(14)	74(15)	76(14)	−24(12)	−17(12)	19(11)
C(15)	48(12)	97(15)	42(10)	−2(10)	−3(9)	−20(11)
C(16)	82(16)	42(11)	73(15)	−9(10)	−12(12)	−4(10)
C(18)	66(11)	37(9)	53(10)	−7(8)	−17(9)	−16(8)
C(19)	78(14)	41(10)	46(11)	−7(8)	−6(10)	−5(10)
C(20)	77(13)	52(11)	43(10)	−5(8)	−18(9)	−21(9)
C(21)	93(17)	40(10)	58(12)	1(9)	−22(12)	−28(10)
C(22)	69(13)	45(11)	41(11)	−11(9)	4(10)	−4(10)
C(24)	130(3)	58(14)	64(14)	−19(11)	12(15)	−36(15)
C(25)	100(2)	73(16)	58(13)	−25(12)	3(13)	−15(14)

TABLE 6 Hydrogen Coordinates ($\times 10^4$) and Isotropic Displacement Parameters ($Å^2 \times 10^3$) for VOAD

	x	y	z	U_{eq}
H(8)	11376	6561	8767	72
H(11)	5072	11647	5269	65
H(13A)	9517	9626	9231	101
H(13B)	11445	8859	8627	101
H(13C)	10376	8313	10003	101
H(14A)	10093	4575	7735	123
H(14B)	10914	4443	8816	123
H(14C)	11888	5012	7421	123
H(15A)	9153	9601	3997	102
H(15B)	8674	11015	4057	102
H(15C)	7487	10561	3550	102

(Continued)

TABLE 6 Continued

	x	y	z	U_{eq}
H(16A)	2329	11722	8316	108
H(16B)	2066	12190	6961	108
H(16C)	3485	12627	7266	108
H(18)	3938	9140	10306	63
H(19)	2524	8455	12336	73
H(21)	4633	4914	11910	76
H(22)	5987	5727	9909	71
H(24A)	2243	4603	15099	133
H(24B)	4175	4404	14142	133
H(24C)	2481	4353	13807	133
H(25A)	1083	6433	15308	127
H(25B)	468	7479	14188	127
H(25C)	2222	7445	14505	127